AN EFFECTIVE STRATEGY FOR REDUCING THE TRUNCATION ERROR IN THE NF–FF TRANSFORMATION WITH HELICOIDAL SCANNING

F. D'Agostino, F. Ferrara, C. Gennarelli, R. Guerriero, G. Riccio
D.I.I.I.E. - University of Salerno, via Ponte Don Melillo, 84084 Fisciano (SA), Italy.

C. Rizzo
MI Technologies Europe, 3 Hither Green Southbourne Emsworth, PO10 8JA,UK.

ABSTRACT

A sophisticated strategy for extrapolating the samples external to the measurement region in the helicoidal scanning is proposed in this paper. It relies on the nonredundant sampling representations of the electromagnetic field and on the optimal sampling interpolation expansions of central type. Such a technique uses the singular value decomposition method for evaluating the outside samples. The estimation of such data allows one to reduce the truncation error affecting the field interpolation in the zone close to the ends of the scanning cylinder, thus giving rise to a more accurate far-field reconstruction. Some numerical tests, assessing the accuracy of the technique and its stability with respect to random errors affecting the data, are reported.

Keywords: Extrapolation, Helicoidal scanning, NF–FF transformations, Nonredundant representations of electromagnetic fields, Truncation error reduction.

1. Introduction

Measurement techniques in the antenna near-field (NF) region play a significant role in the evaluation of far-field (FF) patterns and in the determination of electrical and/or geometrical properties [1]. In particular, the pattern evaluation from NF measurements allows one to overcome those drawbacks which, for electrically large radiating sources, make unpractical to measure the FF data on a conventional FF range.

Among the NF–FF transformation techniques, those employing helicoidal scans allow a remarkable reduction of the time needed for data acquisition by means of continuous and synchronized movements of the positioning systems of the probe and of the antenna under test (AUT). In particular, a uniform circular helix with constant step in z and a nonuniform helix with an elevation step constant in θ have been considered in [2], [3], respectively. In both cases, a nonredundant representation of the voltage data acquired by the measurement probe on the considered helix has been developed by applying the theoretical results on the nonredundant sampling representations of electromagnetic (EM) fields [4]. In addition, the choice of the helix step equal to the corresponding sample spacing needed to interpolate the data along a generatrix has allowed one to obtain the required two-dimensional optimal sampling interpolation (OSI) formula for reconstructing the voltage at any point on the cylinder. It is so possible to determine the NF data needed by the classical probe compensated NF–FF transformation with cylindrical scanning [5].

Unfortunately, the scanning region is always finite, and thus an inevitable truncation error affects the reconstruction in the zones close to its ends. As a consequence, the reconstruction results to be accurate in a zone smaller than the measurement one and this implies a decrease of the angular region wherein an accurate FF reconstruction is attained.

The aim of this work is to develop a sophisticated strategy for extrapolating the samples external to the scanning region. The estimation of such data (otherwise equal to zero in the application of the OSI algorithm) allows one to reduce the truncation error, thus giving rise to a more accurate FF reconstruction. The extrapolation process relies on the knowledge of extra data acquired on very few peripheral rings and makes use of the singular value decomposition (SVD) algorithm [6] for determining the outside data.

2. Nonredundant sampling representation of the probe voltage

Since the voltage measured by a non directive probe has the same effective spatial bandwidth of the field, the aforementioned theoretical results on the nonredundant representation of EM fields [4] can be applied to such a voltage. Accordingly, if the AUT is enclosed in a sphere of radius a and the helix is described by an analytical parameterization $\underline{r} = \underline{r}(\xi)$, it is possible to consider the "reduced probe voltage"

$$\tilde{V}(\xi) = V(\xi)\, e^{j\gamma(\xi)} \tag{1}$$

where $\gamma(\xi)$ is a phase function to be determined. The error, occurring when $\tilde{V}$ is approximated by a spatially bandlimited function, becomes negligible as the bandwidth exceeds the critical value [4]

$$W_\xi = \max_\xi \left[w(\xi) \right] = \max_\xi \left[\max_{\underline{r}'} \left| \frac{\mathrm{d}\gamma(\xi)}{\mathrm{d}\xi} - \beta \frac{\partial R(\xi, \underline{r}')}{\partial \xi} \right| \right] \quad (2)$$

where β is the wavenumber, $\underline{r}'$ denotes the source point and $R(\xi, \underline{r}') = |\underline{r}(\xi) - \underline{r}'|$. Therefore, such an error can be controlled by choosing a bandwidth equal to $\chi' W_\xi$, $\chi' > 1$ being an excess bandwidth factor.

According to the results in [4], a nonredundant sampling representation of the voltage on a helix with constant angular step $\Delta\theta$ (see Fig. 1) can be obtained by using the following expressions for the optimal phase function and parameterization:

$$\gamma(s) = \frac{\beta}{2} \int_0^s \left[\max_{\underline{r}'} \hat{R} \cdot \hat{t} + \min_{\underline{r}'} \hat{R} \cdot \hat{t} \right] \mathrm{d}s \quad (3)$$

$$\xi = \xi(s) = \frac{\beta}{2W_\xi} \int_0^s \left[\max_{\underline{r}'} \hat{R} \cdot \hat{t} - \min_{\underline{r}'} \hat{R} \cdot \hat{t} \right] \mathrm{d}s \quad (4)$$

where s is the arclength of the helix, $\hat{t}$ is the unit vector tangent to it at the observation point P, and $\hat{R}$ is the unit vector from the source point to P.

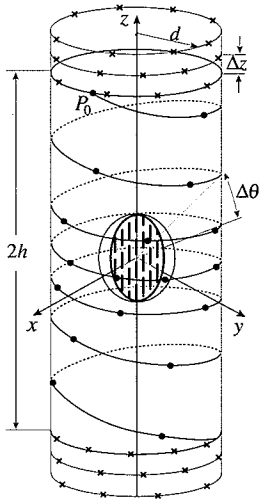

Figure 1 - Helicoidal scanning

The coordinates of P, when imposing the passage of the helix through a given point P_0 of the generatrix at $\phi = 0$, are:

$$\begin{cases} x = d\cos(\varphi - \varphi_i) \\ y = d\sin(\varphi - \varphi_i) \\ z = d\cot\theta \end{cases} \quad (5)$$

where φ_i is the value at P_0 of the angular parameter φ describing the helix, $\theta = k\varphi$, and d is the cylinder radius. Such a helix can be viewed as intersection of the cylindrical surface with the line from the origin to a point moving on a spiral which wraps the sphere of unit radius. In order to allow the two-dimensional interpolation, the helix step $\Delta\theta$ must be equal to the sample spacing needed to interpolate the voltage along a generatrix [7]. Then, the parameter k is such that the step, determined by the consecutive intersections $P(\varphi)$ and $P(\varphi + 2\pi)$ of the helix with the cylinder generatrix, is $\Delta\theta = 2\pi/(2M+1)$, with $M = \mathrm{Int}[\chi M'] + 1$ and $M' = \mathrm{Int}[\chi' \beta a] + 1$. Accordingly, being $\Delta\theta = 2\pi k$, it follows that $k = 1/(2M+1)$. The function $\mathrm{Int}[x]$ gives the integer part of x and $\chi > 1$ is an oversampling factor.

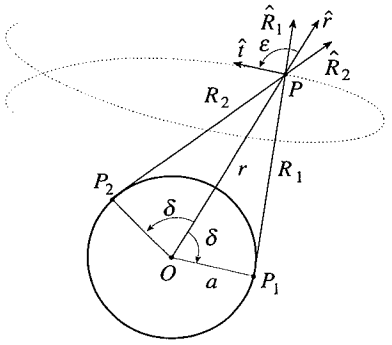

Figure 2 - Geometry in the plane $\hat{r}$, $\hat{t}$

It can be verified that the extreme values of $\hat{R} \cdot \hat{t}$ are determined by considering the intersection of the plane defined by $\hat{t}$ and the unit vector $\hat{r}$ (pointing from the origin to P) with the cone with the vertex at P and the generatrices coincident with the tangents to the source ball (Fig. 2). Denoting by $\hat{R}_{1,2}$ the related unit vectors and by ε the angle between $\hat{r}$ and $\hat{t}$, it results:

$$\left(\hat{R}_1 + \hat{R}_2 \right) / 2 = \hat{r} \sin\delta = \hat{r} \sqrt{1 - a^2/r^2} \quad (6)$$

$$\left(\hat{R}_1 - \hat{R}_2 \right) \cdot \hat{t} \,/ 2 = \cos\delta \sin\varepsilon = (a/r) \sin\varepsilon \quad (7)$$

By substituting (6) into (3) and taking into account that $\mathrm{d}r = \hat{r} \cdot \hat{t}\, \mathrm{d}s$, we obtain:

$$\gamma = \beta \int_0^r \sqrt{1 - a^2/r^2}\, \mathrm{d}r = \beta \sqrt{r^2 - a^2} - \beta a \cos^{-1}\left(\frac{a}{r} \right) \quad (8)$$

On the other hand

$$\mathrm{d}s = \left(d / \sin^2 k\varphi \right) \sqrt{k^2 + \sin^4 k\varphi}\ \mathrm{d}\varphi \quad (9)$$

and

$$\sin\varepsilon = \sqrt{1 - (\hat{r} \cdot \hat{t})^2} \quad (10)$$

wherein

$$\hat{r} \cdot \hat{t} = -k \cos k\varphi \Big/ \sqrt{k^2 + \sin^4 k\varphi} \quad (11)$$

By taking into account (10) and substituting relations (7) and (9) in (4), it results:

$$\xi = \frac{\beta a}{W_\xi} \int_0^{\varphi} \sqrt{k^2 + \sin^2 k\varphi'}\, \mathrm{d}\varphi' \tag{12}$$

As can be seen, the optimal parameter ξ is proportional to the curvilinear abscissa along the spiral wrapping the sphere of unit radius. Since such a spiral is a closed curve, it is convenient to choose the bandwidth W_ξ such that ξ covers a 2π range when the whole curve on the sphere is described. As a consequence,

$$W_\xi = \frac{\beta a}{\pi} \int_0^{(2M+1)\pi} \sqrt{k^2 + \sin^2 k\varphi'}\, \mathrm{d}\varphi' \tag{13}$$

In the light of these results, the voltage at any point of the helix can be reconstructed via the OSI formula:

$$\tilde{V}(\xi) = \sum_{n=n_0-q+1}^{n_0+q} \tilde{V}(\xi_n)\, \Omega_{N''}(\xi - \xi_n)\, D_N(\xi - \xi_n) \tag{14}$$

where $n_0 = \mathrm{Int}\big((\xi - \xi(\varphi_i))/\Delta\xi\big)$ is the index of the sample nearest (on the left) to the output point, $2q$ is the number of retained samples and

$$\xi_n = \xi(\varphi_i) + n\Delta\xi = \xi(\varphi_i) + 2\pi n/(2N+1) \tag{15}$$

$$N = \mathrm{Int}(\chi N') + 1 \; ; \qquad N' = \mathrm{Int}(\chi' W_\xi) + 1 \tag{16}$$

Moreover,

$$D_N(\xi) = \frac{\sin\big((2N+1)\xi/2\big)}{(2N+1)\sin(\xi/2)} \tag{17}$$

$$\Omega_{N''}(\xi) = \frac{T_{N''}\Big[2\big(\cos(\xi/2)/\cos(\xi_0/2)\big)^2 - 1\Big]}{T_{N''}\Big[2/\cos^2(\xi_0/2) - 1\Big]} \tag{18}$$

are the Dirichlet and Tschebyscheff Sampling functions, respectively, $T_{N''}(\cdot)$ being the Tschebyscheff polynomial of degree $N'' = N - N'$ and $\xi_0 = q\Delta\xi$.

Expansion (14) can be properly employed to evaluate the voltage at any point P on the cylinder. In fact, it allows the evaluation of the "intermediate" samples, namely the voltage values at the intersection points of the helix with the generatrix passing through P. Once these samples have been determined, because of the particular choice of $\Delta\theta$, the voltage can be reconstructed via the OSI expansion:

$$\tilde{V}(\theta,\phi) = \sum_{m=m_0-p+1}^{m_0+p} \tilde{V}(\theta_m)\, D_M(\theta - \theta_m)\, \Omega_{M''}(\theta - \theta_m) \tag{19}$$

where $\theta_m = \theta_m(\phi) = \theta(\varphi_i) + k\phi + m\Delta\theta = \theta_0 + m\Delta\theta$, $m_0 = \mathrm{Int}\big[(\theta - \theta_0)/\Delta\theta\big]$, $M'' = M - M'$, $\tilde{V}(\theta_m)$ are the intermediate samples, and the other symbols have the same meaning as in (14).

3. NF–FF transformation

The algorithm described in the previous Section can be applied to efficiently reconstruct the NF data, needed for the classical probe compensated NF–FF transformation [5], from the voltage samples acquired on a helix wrapping a cylinder.

As previously stated, the scanning region is always finite, and thus an inevitable truncation error affects the reconstruction of the NF data in the zones close to the ends. Accordingly, the reconstruction results to be accurate in a zone smaller than the measurement one. To overcome this drawback, a sophisticated strategy for extrapolating the samples external to the scanning region will be developed in the next Section.

As shown in [5], the modal coefficients a_υ and b_υ of the cylindrical wave expansion of the field radiated by AUT are related to: a) the two-dimensional Fourier transforms of the output voltages V and V' of the probe for two independent sets of measurements (the probe is rotated 90° about its longitudinal axis in the second set); b) the modal coefficients of the cylindrical wave expansion of the field radiated by the probe and the rotated probe, when used as transmitting antennas. Once the modal coefficients are determined, the FF components of the electric field in the spherical coordinate system (R,Θ,Φ) can be evaluated by:

$$E_\Theta = -\mathrm{j}2\beta \frac{\mathrm{e}^{-\mathrm{j}\beta R}}{R} \sin\Theta \sum_{\upsilon=-\infty}^{\infty} \mathrm{j}^\upsilon b_\upsilon(\beta\cos\Theta)\mathrm{e}^{\mathrm{j}\upsilon\Phi} \tag{20}$$

$$E_\Phi = -2\beta \frac{\mathrm{e}^{-\mathrm{j}\beta R}}{R} \sin\Theta \sum_{\upsilon=-\infty}^{\infty} \mathrm{j}^\upsilon a_\upsilon(\beta\cos\Theta)\mathrm{e}^{\mathrm{j}\upsilon\Phi} \tag{21}$$

As well-known, the summations in these last relations can be efficiently performed via the fast Fourier transform (FFT) algorithm.

4. Extrapolation algorithm

This Section deals with the strategy for extrapolating the NF samples external to the scanning region. In order to explain the methodology, let us consider the upper half of the measurement cylinder. Besides the regular samples acquired via the helicoidal scanning, let us assume the knowledge of the probe voltages on J rings spaced at a fixed step Δz, from the top of the cylinder. On each of these rings, the extra samples are known at the points specified by

$$\phi_{n,j} = n\Delta\phi_j = 2n\pi/(2N_j+1) \tag{22}$$

where

$$N_j = \mathrm{Int}(\chi N'_j)+1 \; ; \quad N'_j = \mathrm{Int}(\chi^* W_{\phi_j})+1 \tag{23}$$

$$W_{\phi_j} = W_\phi(\theta_j) = \beta a \sin\theta_j \tag{24}$$

$$\chi^* = 1+(\chi'-1)\left[\sin\theta_j\right]^{-2/3} \tag{25}$$

$$\theta_j = \tan^{-1}\left(d/(h+j\Delta z)\right) \qquad j = 1,\ldots,J \tag{26}$$

On each cylinder generatrix fixed by ϕ, the reduced voltage at the intersection points $P(\theta_j,\phi)$ with the extra rings can be evaluated via the OSI expansion [4]

$$\tilde{V}(\theta_j) = \tilde{V}(\theta_j,\phi) =$$

$$= \sum_{n=n_0-q+1}^{n_0+q} \tilde{V}(\theta_j,\phi_{n,j})\,\Omega_{N''_j}(\phi-\phi_{n,j})\,D_{N_j}(\phi-\phi_{n,j}) \tag{27}$$

where $2q$ is the number of retained samples along ϕ, $n_0 = \mathrm{Int}(\phi/\Delta\phi_j)$, and $N''_j = N_j - N'_j$.

When applying (19) to each of the points $P(\theta_j,\phi)$, just p unknown outside samples $\tilde{V}(\theta_m)$ are always involved, since the other can be reconstructed via (14). Accordingly, by centring the OSI formula (19) on the first known intermediate sample at θ_0, so that the index m assumes negative values for the external samples to be estimated, for each $j = 1,\ldots,J$ we get:

$$\tilde{V}(\theta_j) - \sum_{m=0}^{p} \tilde{V}(\theta_m) D_M(\theta_j-\theta_m)\,\Omega_{M''}(\theta_j-\theta_m) =$$

$$= \sum_{m=-\bar{p}}^{-1} \tilde{V}(\theta_m) D_M(\theta_j-\theta_m)\,\Omega_{M''}(\theta_j-\theta_m) \tag{28}$$

where $\bar{p} \le p$ is the number of external samples to be estimated. These J equations can be rewritten in matrix form as $\underline{\underline{A}}\,\underline{x} = \underline{b}$, where $\underline{b}$ is the sequence of the known terms, $\underline{\underline{A}}$ is the $J \times \bar{p}$ matrix, whose elements $A_{jm} = D_M(\theta_j-\theta_m)\,\Omega_{M''}(\theta_j-\theta_m)$ are given by the weight functions in the considered OSI expansion and $\underline{x}$ is the sequence of the unknown outside samples $\tilde{V}(\theta_m)$, with $m = -\bar{p},\ldots,-1$. A solution, which is the best approximation in the least squares sense of the linear system (28), can be obtained by using the SVD technique. A quite similar procedure can be used for extrapolating the samples external to the lower end of the cylinder.

Once the outside samples relevant to the considered generatrix have been estimated, the voltage values at any point on it can be evaluated via (19).

It must be stressed that the matrix $\underline{\underline{A}}$ depends on the samples position on the considered generatrix. In fact, the z-coordinates of the regular samples (those obtained as intersection between the generatrix and the helix) decrease as the azimuthal angle ϕ increases. In order to obtain a regularized solution of the linear system (28), a Tikhonov regularization approach can be applied [6]. Such a solution corresponds to minimize the following functional:

$$\left\|\underline{\underline{A}}\,\underline{x}-\underline{b}\right\|_2^2 + \alpha^2\left\|\underline{x}\right\|_2^2 \tag{29}$$

α being the regularization parameter. Thus, we can write the regularized solution $\underline{x}_{\mathrm{reg}}$ and the corresponding residual vector $\underline{b}-\underline{\underline{A}}\,\underline{x}_{\mathrm{reg}}$ in term of the SVD of $\underline{\underline{A}}$ in the generic form

$$\underline{x}_{\mathrm{reg}} = \sum_{i=1}^{\bar{p}} f_i \frac{\underline{u}_i^{\mathrm{H}}}{\sigma_i}\underline{v}_i \tag{30}$$

$$\underline{b}-\underline{\underline{A}}\,\underline{x}_{\mathrm{reg}} = \sum_{i=1}^{\bar{p}}(1-f_i)\underline{u}_i^{\mathrm{H}}\underline{b}\;\underline{u}_i + \sum_{i=1}^{\bar{p}} f_i \underline{u}_i^{\mathrm{H}}\underline{b}\;\underline{u}_i \tag{31}$$

where H denotes the conjugate transposition operator, σ_i, with $i = 1,\ldots,\bar{p}$, are the singular values of $\underline{\underline{A}}$, ordered from the maximum to the minimum value, $f_i = \sigma_i^2/(\sigma_i^2+\alpha^2)$ are the corresponding filter factors, and $\underline{u}_i$, $\underline{v}_i$ are the left and right singular vector of $\underline{\underline{A}}$, respectively [6]. The choice of the optimal parameter α to be used can be made by using the L-curve. Such a curve is a plot in log-log scale for all valid regularization parameters of the norm of the regularized solution $\underline{x}_{\mathrm{reg}}$, versus the corresponding residual norm of $\underline{b}-\underline{\underline{A}}\,\underline{x}_{\mathrm{reg}}$. The L-curve displays the compromise between the minimization of these two quantities, which is the heart of any regularization method. With reference to the Tikhonov regularization, the best compromise is represented by the distinct corner separating the vertical and the horizontal part of the curve.

5. Numerical tests

The reported numerical tests refer to a uniform planar array of 0.6 λ spaced elementary Huygens sources polarized along the z axis and lying in an elliptical zone on the plane $y = 0$, with major and minor semiaxes equal to 16.2 λ and 12 λ, respectively (λ being the wavelength). An open-ended WR-90 rectangular waveguide, operating at the frequency of 10 GHz, is chosen as probe. The radius d of the cylinder is 18λ and its height $2h$ is 140λ. According to the described sampling representation, $J = 6$ extra rings have been acquired and added at both cylinder ends. They are spaced at $\Delta z = 1\lambda$. It is worthy to note that, on each side of a given generatrix, the number of outside

samples is $\bar{p} = 6$. A Tikhonov regularization approach has been applied to obtain the best estimation of the outside samples for all the considered generatrices. We have assumed $p = 17$ in the extrapolation process of the outside samples, whereas $q = 6$ has been adopted both in (14) and in (27) to obtain the involved known samples and the extra data, respectively. It must be stressed that the SVD is applied to a small matrix with a negligible computational effort.

Figure 3 shows the amplitude of the output voltage V on the cylinder generatrix at ϕ = 90°. It has been reconstructed without using the extrapolation process and putting the outside samples equal to zero. As can be seen in Fig. 4, by using the proposed estimation procedure, the reconstruction is very accurate not only in the whole measurement region, but also in a zone outside it. It is worthy to note that, in both cases, $p = 6$ has been adopted when applying (19) for the reconstruction. A further reconstruction example relevant to the generatrix at ϕ = 120° is reported in Fig. 5. In order to assess more quantitatively the effectiveness of the approach, the maximum and mean-square reconstruction errors have been evaluated by comparing, on a cylindrical grid of height 150λ (slightly greater than the scan region), the exact values of V and those reconstructed with and without the estimated outside samples. Figure 6 shows such errors, normalized to the voltage maximum value on the cylinder. As can be seen, the errors evaluated by considering the estimated samples decrease quite rapidly until very low levels are reached. On the contrary, those obtained without considering them saturate to constant values, due to the truncation error present in the zones close to the ends. The algorithm stability has been assessed (see Fig. 7) by adding random errors to the exact samples. These errors simulate a background noise, bounded to Δa (dB) in amplitude and with arbitrary phase, and an uncertainty on the data of $\pm\Delta a_r$ (dB) in amplitude and $\pm\Delta\alpha$(degrees) in phase.

Figure 8 reports the antenna FF pattern in the E-plane reconstructed by taking into account the estimated samples. As can be seen, the exact and recovered fields are practically indistinguishable. A zoom of the far out side lobe region relevant to the reconstruction obtained without and with the estimated samples is reported in Fig. 9 and 10, respectively. As can be

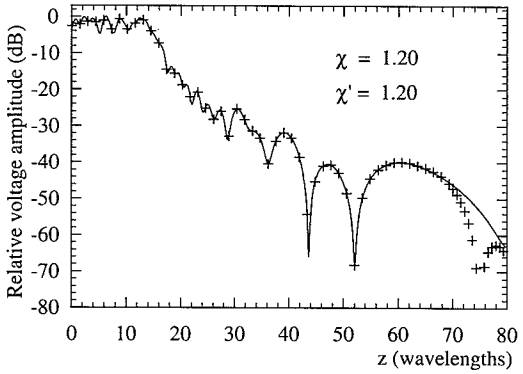

Figure 3 - Amplitude of the probe voltage V on the generatrix at ϕ =90°. Solid line: exact. Crosses: reconstructed without estimated outside samples.

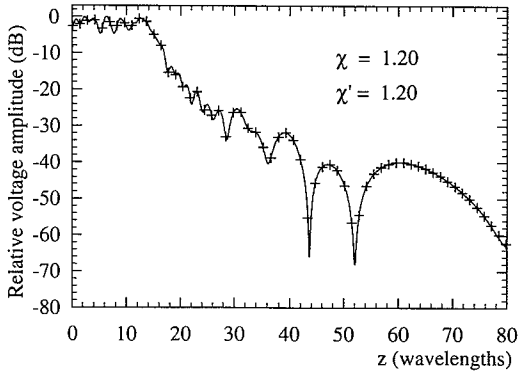

Figure 4 - Amplitude of the probe voltage V on the generatrix at ϕ =90°. Solid line: exact. Crosses: reconstructed with estimated outside samples.

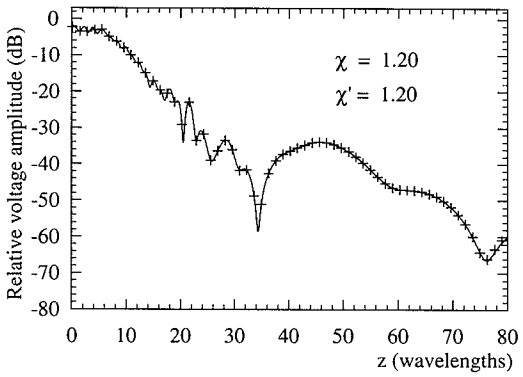

Figure 5 - Amplitude of the probe voltage V on the generatrix at ϕ =120°. Solid line: exact. Crosses: reconstructed with estimated outside samples.

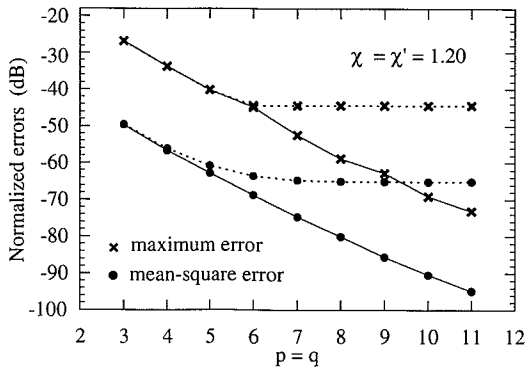

Figure 6 - Normalized reconstruction errors. Dashed line: without estimated outside samples. Solid line: with estimated outside samples.

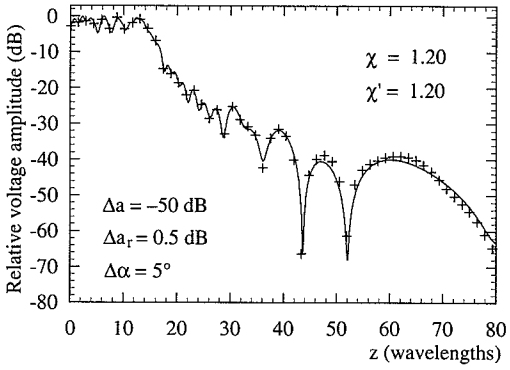

Figure 7 - Amplitude of the probe voltage V on the generatrix at ϕ =90°. Solid line: exact. Crosses: reconstructed with estimated outside samples from error affected data.

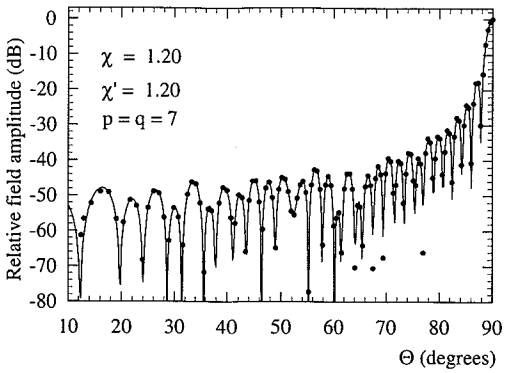

Figure 8 - E-plane pattern. Solid line: exact. Dots: reconstructed via the NF–FF transformation with estimated outside samples.

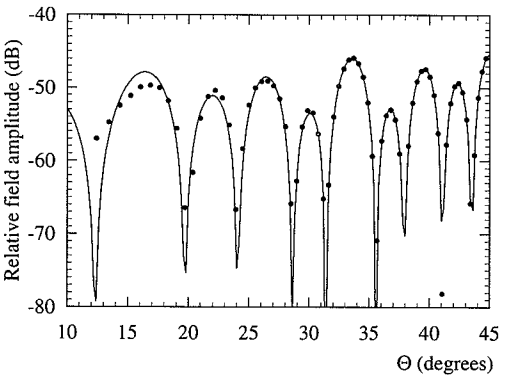

Figure 9 - Zoom of the E-plane pattern. Solid line: exact. Dots: reconstructed via the NF–FF transformation without estimated outside samples.

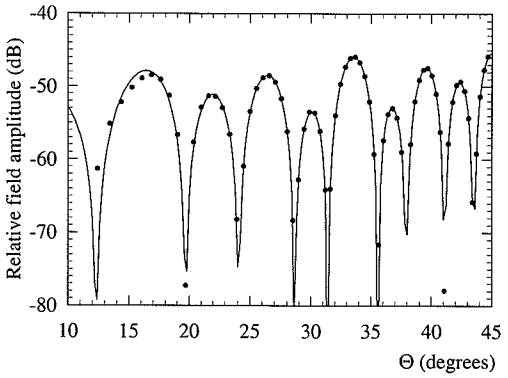

Figure 10 - Zoom of the E-plane pattern. Solid line: exact. Dots: reconstructed via the NF–FF transformation with estimated outside samples.

seen, the reconstruction obtained by considering the estimated samples is more accurate, thus assessing the effectiveness of the proposed technique.

It is worthy to note that the number of employed samples for reconstructing the NF data on the considered cylinder ($2h = 160\lambda$) is 27 775, less than half of that (60 103) required by the approach in [2] and significantly less than that (81 920) needed by the approach in [5]. In particular, the number of "extra" samples on the rings (at the ends of the scanning cylinder) is 1112.

6. REFERENCES

[1] C.Gennarelli, G.Riccio, F.D'Agostino, and F.Ferrara, *Near-field – far-field transformation techniques*, CUES, Salerno, Italy, 2004.

[2] O.M.Bucci, C.Gennarelli, G.Riccio, and C.Savarese, "Probe compensated NF–FF transformation with helicoidal scanning," *J. Electromagn. Waves Appl.*, vol. 14, pp. 531-549, 2000.

[3] O.M.Bucci, C.Gennarelli, G.Riccio, and C.Savarese, "Nonredundant NF–FF transformation with helicoidal scanning," *J. Electromagn. Waves Appl.*, vol. 15, pp. 1507-1519, 2001.

[4] O.M.Bucci, C.Gennarelli, and C.Savarese, "Representation of electromagnetic fields over arbitrary surfaces by a finite and nonredundant number of samples," *IEEE Trans. Antennas Propagat.*, vol. 46, pp. 351-359, 1998.

[5] W.M.Leach Jr. and D.T.Paris, "Probe compensated NF measurements on a cylinder," *IEEE Trans. Antennas Propagat.*, vol. AP-21, pp.435-445, 1973.

[6] P.C.Hansen, *Rank-deficient and discrete ill-posed peoblems*, SIAM, Philadelphia, 1998.

[7] O.M.Bucci, C.Gennarelli, G.Riccio, C.Savarese, and V.Speranza, "Non redundant representation of the electromagnetic fields over a cylinder with application to the near-field–far-field transformation," *Electromagnetics*, vol. 16, pp. 273-290, 1996.